Geophysical Research Letters®

Key Points:

- We present the first disk measurements of Mars discrete aurora in the EUV end FUV, with the oxygen feature at 130.4 nm being the brightest
- Auroras are detected in ~75% of nightside images and are more likely where crustal fields are either very weak or both strong and vertical
- An elongated, sinuous discrete aurora is discovered, extending far into the nightside. It may be related to the magnetotail current sheet

First Synoptic Images of FUV Discrete Aurora and Discovery of Sinuous Aurora at Mars by EMM EMUS

Robert J. Lillis[1] , **Justin Deighan[2]** , **David Brain[2]** , **Matthew Fillingim[1]**, **Sonal Jain[2]** , **Michael Chaffin[2]** , **Scott England[3]**, **Greg Holsclaw[2]** , **Krishnaprasad Chirakkil[2,4]** , **Hessa Al Matroushi[5]** , **Fatma Lootah[5]** , **Hoor Al Mazmi[6]** , **Ed Thiemann[2]** , **Frank Eparvier[2]** , **Nick Schneider[2]** , and **Shannon Curry[1]**

[1]Space Sciences Laboratory, University of California Berkeley, Berkeley, CA, USA, [2]Laboratory for Atmospheric and Space Physics, University of Colorado, Boulder, CO, USA, [3]Department of Aerospace and Ocean Engineering, Virginia Institute of Technology, Blacksburg, VA, USA, [4]Space and Planetary Science Center, Khalifa University, Abu Dhabi, UAE, [5]Mohammed Bin Rashid Space Center, Dubai, UAE, [6]United Arab Emirates Space Agency, Abu Dhabi, UAE

Abstract We present the first measurements of Mars discrete aurora in the extreme ultraviolet (<110 nm) and the first synoptic aurora images in the far ultraviolet (110–180 nm). Auroral emission is detected in >75% of nightside images, with patterns shifting visibly over 15–20 min. Aurora is observed most frequently in regions of open magnetic topology (where crustal magnetic fields are very weak and/or vertical), with the brightest aurora where crustal fields are strongest. We present the first disk-averaged spectrum of discrete aurora, with several O, C, and CO features as expected for electron impact primarily on CO_2. We categorize discrete auroral morphology into three types: crustal field aurora, non-crustal field patchy aurora, and a new type we call "sinuous" aurora, an elongated serpentine structure that stretches thousands of kilometers into the nightside from near midnight in the northern hemisphere. These observations point to a highly dynamic environment in Mars' magnetotail.

Plain Language Summary In this study, we present near-global images of localized aurora on Mars and the first measurements of these aurora at very short ultraviolet wavelengths (<110 nm). They are caused by energetic electrons from the solar wind smashing into Mars' upper atmosphere. We find auroras in >75% of images, with their patterns shifting visibly over 15–20 min. They are observed most frequently in regions where magnetic fields are very weak or both strong and vertical, with the brightest aurora where magnetic fields are strongest. We present the first disk-averaged spectrum of these auroras, showing features expected for electrons striking CO_2 (the most abundant gas in Mars' atmosphere). We categorize discrete auroral patterns into three types: those near strong vertical crustal magnetic field, patchy aurora near very weak crustal fields, and a new type we call "sinuous," an elongated serpentine structure that stretches thousands of kilometers into the nightside from near midnight in the northern hemisphere. These observations point to a highly dynamic environment in Mars' nightside space environment.

1. Introduction

Martian discrete auroras are spatially confined regions of photon emission caused by the precipitation of suprathermal (>~5 eV) electrons into Mars' nightside upper atmosphere. Electron impact causes electronic excitations of atoms and molecules, whose decay releases ultraviolet and visible photons. Discrete aurorae were discovered by the SPICAM UV spectrometer (Bertaux et al., 2005) onboard Mars Express (MEx) and were characterized by small spatial scales, a tendency to form in regions of strong vertical crustal magnetic fields, and an association with sheath and magnetotail electrons that have been energized (Brain et al., 2006; Leblanc et al., 2006, 2008). Discrete aurora is thus distinct from the other two types of Mars aurora, namely diffuse aurora [caused by global precipitation of solar energetic electrons and protons (Gerard et al., 2017; Nakamura et al., 2022; Schneider et al., 2015)] and proton aurora [caused by precipitation of solar wind protons directly into the dayside upper atmosphere (Deighan et al., 2018; Hughes et al., 2019; Ritter et al., 2018; Chaffin et al., 2022)].

SPICAM observed 16 nadir detections (Gérard et al., 2015) and three limb detections (Soret et al., 2016) of discrete aurora on 9 out of 113 orbits selected to be near strong crustal magnetic fields, whereas the Imaging Ultraviolet Spectrograph (IUVS) on the MAVEN spacecraft has detected more than 200 discrete aurorae between 2015 and 2020 (Schneider et al., 2021; Soret et al., 2021). The spectral signature of the detected discrete aurora

Investigation: Justin Deighan, Matthew Fillingim, Sonal Jain, Michael Chaffin, Scott England, Greg Holsclaw, Krishnaprasad Chirakkil, Fatma Lootah, Hoor Al Mazmi
Methodology: Justin Deighan, Sonal Jain
Project Administration: Hessa Al Matroushi
Software: Justin Deighan
Validation: Justin Deighan
Writing – review & editing: Michael Chaffin, Krishnaprasad Chirakkil, Nick Schneider

thus far has been not only in the mid-ultraviolet (MUV), specifically the CO Cameron bands, the 297.2 nm O emission, and the 289 nm CO_2^+ UV doublet (Gérard et al., 2015; Leblanc et al., 2006; Soret et al., 2021) but also in the far ultraviolet (FUV) at 130.4 nm and the CO_4 PG bands (135–170 nm) (Soret et al., 2016). Different behavior is observed within, and away from, Mars' strong crustal magnetic field region in the southern hemisphere. Within this region, discrete aurora occurs more frequently on the dusk side and for westward interplanetary magnetic field (IMF) directions (Schneider et al., 2021) with no significant dependence on local time or IMF direction in other regions. Xu et al. (2022) showed that accelerated electron events share the same characteristics (locations, crustal field, etc.) as the auroral events, establishing a causal connection. Girazian et al. (2022) showed that high solar wind pressures increase the IUVS auroral detection frequency but not emission brightness. Finally, Fang et al. (2022) used global plasma modeling to predict that aurora should occur more frequently (a) in small-scale patches near strong crustal fields (consistent with Schneider et al. (2021)) and (b) when coronal mass ejections (CMEs) impact Mars (consistent with Girazian et al. (2022)).

Due to sensitivity and data coverage limitations, all investigations of discrete aurora have, up to now, concerned a relatively small number of isolated detections. The locations and favorable conditions of discrete aurora have been determined only in a statistical sense, from several years of observations. Despite the substantial amount we have learned, with these limitations we have had little insight into global occurrence and instantaneous patterns of discrete aurora.

2. Data Set

2.1. The EMUS Instrument

EMUS is an EUV/FUV spectrometer mounted on the instrument deck of the EMM Hope Orbiter. Light entering its narrow 0.6° × 11° aperture (or "slit") is focused by a spherical mirror onto a diffraction grating which splits the light into its spectral components, resulting in a two-dimensional image (1 spatial × 1 spectral) on a micro-channel plate detector. Photon counts in each pixel are recorded in 7-s integrations. Hope orbits every ∼55 hr in a 20,000 × 43,000 km (6.9 × 13.7 Mars radii) science orbit inclined at 25°, providing near-complete geographic and diurnal coverage of Mars every ∼10 days (Amiri et al., 2022). Holsclaw et al. (2021) describes in detail the EMUS instrument and its science goals and data collection modes.

2.2. Creating Images of Mars FUV Emission

In this study, we use data from EMUS's OS-2 collection mode, designed to study Mars' dayside and nightside disk and inner corona (<1.6 Mars radii). In this mode, as the slit moves across the disk, each integration produces a line of rectangular spatial pixels (each with its own FUV spectrum), with significant spatial overlap between adjacent integrations. For each swath, the corners of each spatial pixel are mapped to a grid of geographic pixels. Thus, each geographic pixel is fully or partially "painted over" by multiple instrument spatial pixels (as the slit moves across the disk), whose contributions are averaged, weighting by the fraction of that geographic pixel covered by each spatial pixel. For a given image swath, we can thus make an emission map (like those in Figures 1a and 1b) for any wavelength range from ∼85 to 180 nm.

For this study, we project this map onto a sphere from the perspective of the orbiter's position. Depending on Hope's distance from Mars, two or three parallel swaths comprise one OS-2 observing sequence. Swaths can be "stitched" together to make an image like Figure 1c. Note we also use data from the OS-R mode, starting in December 2021, whereby EMUS "rides along" with observations from the EMIRS instrument (Edwards et al., 2021), performing a single swath covering most, but not always all, of the disk (see Figures 1f and 1g). Figure 1 shows examples of three primary types of discrete aurora (crustal, patchy, and sinuous) seen in this data set; we discuss their morphologies in Section 4. This study concerns data collected between 23 April 2021 and 28 February 2022, totaling 565 observing sequences, of which 417 were collected when the spacecraft SZA >60°, that is, with a clear view of a significant portion of the nightside.

2.3. Sources of 130.4 nm Nightside Emission

In this data set, the brightest emission displaying coherent auroral patterns (like those in Figure 1) is the atomic oxygen 130.4 nm triplet, caused by decay of the $^3S_1$ excited state of oxygen to the ground state ($^3P_2$). This excited
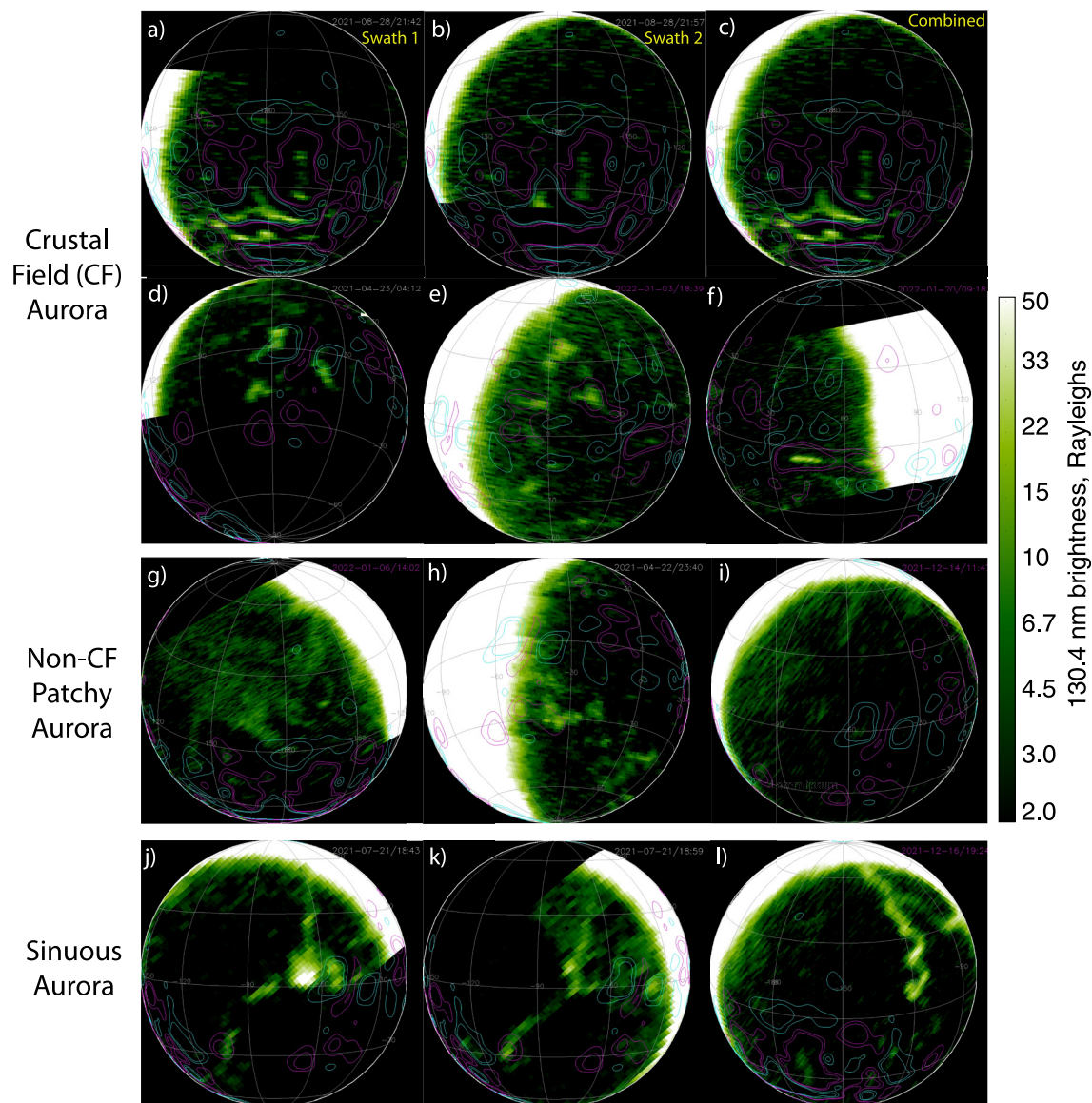
Figure 1. Images of 130.4 nm emission. Panels (a) and (b) show adjacent imaging swaths on 28 August 2021, collected 15 min apart. Panel (c) shows the combined image, averaging the two swaths. Panels (c)–(f) are typical examples of crustal field aurora, panels (g)–(i) are examples of patchy non-crustal field aurora, and panels (j)–(l) are examples of sinuous aurora, with panels j and k taken 16 min apart. Pink and cyan represent positive and negative 10 and 20 nT contours of the vertical (i.e., radial) component of Mars' crustal magnetic fields at 400 km altitude (according to the model of Langlais et al. (2019)).

state has two sources: (a) electron impact causing excitation of O atoms and dissociative excitation of CO and CO_2 molecules in the Mars thermosphere that result in excited O atoms and (b) resonance scattering of solar photons from the same triplet by O atoms. Therefore, when viewing the Martian nightside at 130.4 nm (Figure 1), the former reflects the auroral process that is the focus of this study, while the latter reflects multiple photon scattering in the thermosphere across the terminator from the dayside, plus direct scattering of sunlit oxygen in Mars' exosphere along the line of sight to each pixel. This latter component forms a background for our observations of aurora and can be seen in the "bleeding over" from the dayside (i.e., 130.4 nm dayglow emission) and occasional "streaky" features deeper into the nightside visible in the upper middle part of Figure 1b.

In an attempt to minimize this background while still retaining sufficient coverage, we choose a minimum solar zenith angle (SZA) of 120° for pixels we consider to be "nightside." Thus, all valid pixels are in darkness below 675 km, limiting resonance fluorescence background only to the tenuous hot O exosphere and relatively rare multiple photon scattering events (Deighan et al., 2015).
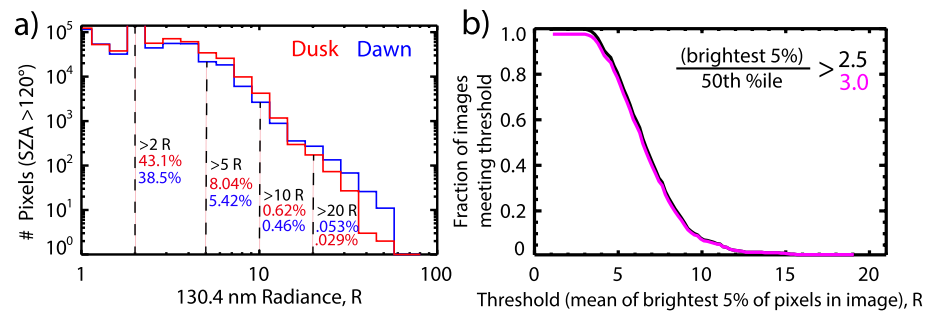
Figure 2. Auroral brightness at 130.4 nm. (a) Histogram of emission from all nightside (SZA >120°) pixels, divided into pre-midnight (dusk, red) and post-midnight (dawn, blue). Labels show the fraction of dawn/dusk pixels brighter than 2, 5, 10, and 20 R (b) Fraction of images where the auroral brightness metric (i.e., mean of brightest 5% of nightside pixels in the image) is brighter than the abscissa (*x*-axis) and where this metric is more than 2.5 (black) and 3.0 (pink) times the 50th percentile (i.e., median) background metric (described in Supporting Information S1).

The choice of a 2 R color threshold for these images is guided by the desire to show faint-but-real auroral features while avoiding more numerous background streaky features. As seen in Figure S1 (Supporting Information S1), a higher choice may be appropriate for images with higher backgrounds.

3. Discrete Aurora Statistical Behavior

It is instructive to examine the distribution of all ~1.9 million nightside (i.e., SZA >120°) pixels at 130.4 nm in our dataset. The fraction brighter than (2, 3, 5, 10, 15, 20) R is (40.8, 21.0, 6.74, 0.54, 0.098, 0.041)%, respectively. Due to variable background signals (see Supporting Information S1), pixels below 5 R cannot be confidently attributed to discrete aurora without visual inspection of a particular image. Figure 2a shows histograms of 130.4 nm emission, divided into dusk (926,364 pixels) and dawn (919,294 pixels) sides. We note that dawn side pixels are 30% less likely than dusk side pixels to be brighter than 5 R and 26% less likely to be brighter than 10 R, showing that auroras are generally brighter before midnight than after, consistent with Schneider et al. (2021). Thresholds above 10 R suffer from small number statistics, whereby a small number of dawnside very bright auroral features (including those in Figure 1l), contain enough pixels to dominate the local time statistics.

One of the primary topics of interest for previous studies has been the frequency with which discrete aurora occur. There are two possible definitions of occurrence frequency: (a) observation occurrence, that is, how often aurora is seen anywhere on the nightside in a given image and (b) geographic occurrence, that is, how often aurora occurs in a given geographic location (detection depends on location because the geographically fixed crustal magnetic fields guide electrons toward or away from certain regions). These two definitions of occurrence are discussed below.

3.1. Observation Occurrence

To make a quantitative estimate of auroral observation occurrence, we choose to define our metric for auroral brightness in a given image as the mean of the brightest 5% of nightside pixels in each image. Let us define auroral detection in a given image as this brightness metric being >5 R and at least three times higher than the background metric (that is, the median of all nightside pixels, see Text in Supporting Information S1). Then Figure 2b demonstrates that aurorae are detected in 77% of images, with auroral brightness metrics above 7 R, 10 R, and 15 R present in 40%, 7.3%, and 1.3% of images, respectively.

We would like to compare this detection frequency with published work based on MEx and MAVEN observations. MAVEN IUVS detected aurora on 196 of 4220 total nightside orbits (4.6 ± 0.3%) (Schneider et al., 2021), whereas MEx SPICAM detected aurora on 12 of 143 orbits (8.4 ± 2.4%) though these orbits were specifically selected for strong crustal fields (Gérard et al., 2015; Soret et al., 2016). However, a meaningful comparison is not possible for two reasons. First, EMUS's aurora detections are at a different wavelength (O 130.4 nm in the FUV vs. Cameron bands and CO_2^+ UV doublet in the MUV) with different detection sensitivity and different sources of background. Second, EMUS views a significant fraction of the night hemisphere in every observing
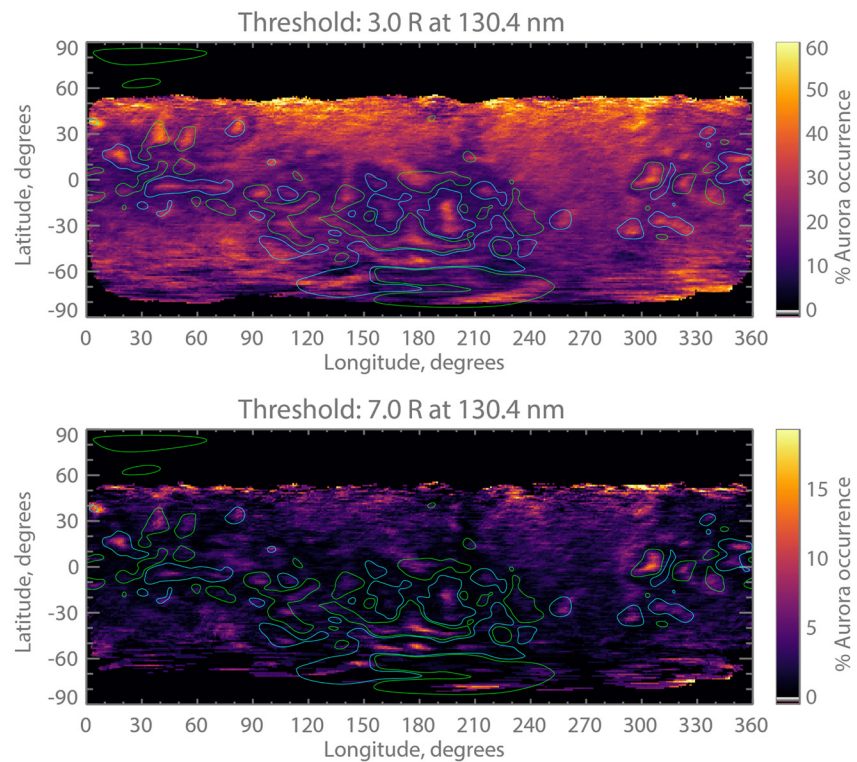
Figure 3. Geographic occurrence rate of discrete aurorae, using emission thresholds of 3 and 7 R. Green and blue contours are the −10 and 10 nT levels of radial crustal magnetic field strength at 400 km altitude from the model of Langlais et al. (2019).

sequence, that is, a much larger area than a single orbit of either MAVEN or MEx saw in limb or nadir mode close to periapsis.

3.2. Geographic Occurrence

The occurrence rate of discrete aurora in a given geographic region is calculated as a fraction. The denominator is the number of instances where an EMUS spatial pixel overlaps with the region, while the numerator is the number of those pixels where the 130.4 nm emission exceeds some threshold. Maps of this geographic occurrence are shown in Figure 3, where each region is a 1° by 1° pixel, along with −10 and 10 nT contours of the radial (i.e., vertical) component of crustal magnetic field. It is clear that discrete aurorae in general are more common in regions where crustal fields are either primarily vertical or weak. This is to be expected as these are also the same regions where magnetic topology is more likely to be "open" (i.e., field lines connected the atmosphere at one end and to the magnetotail/solar wind at the other end) (Brain et al., 2007), allowing solar wind electrons access to the atmosphere, from which impact excitation causes aurorae. Where radial fields are strong (approximately inside the contours), they dominate over the induced magnetotail; horizontal strong fields deny electrons access to the atmosphere while vertical strong fields ensure access. In contrast, where the crustal fields are weak, the magnetotail field dominates and thus topology is often "open," accounting for the high auroral occurrence where the crustal field is the weakest (Lillis et al., 2008). Indeed this map is morphologically quite similar to the map of open field probability published by Brain et al. (2007).

It is also worth noting that bright aurora (>7 R) are more likely in the strongest crustal field region at approximately 180°E, 45°S, referred to as the "sailboat" by previous authors. This is consistent with the work of Schneider et al. (2021), who found the highest detection likelihood in this region with MAVEN IUVS, which had a higher detection limit than EMUS.

4. Morphologies of Discrete Aurora

Although Mars discrete aurora have been detected and studied for ~17 years, each instance has been a point detection, that is, a highly localized "patch" of emission because no global imager existed. EMM's high orbit, combined with EMUS's sensitivity, provides a truly unprecedented perspective on this phenomenon, that is, a synoptic view where a large fraction of a hemisphere is sampled over ~15–45 min. This lets us study the broad-scale morphologies of Mars' discrete aurora. Although there are many varied shapes and patterns in the EMM aurora data set, here we will focus on three of the most common and, in our view, interesting.

The first is a common pattern we call "crustal field aurora" as it observed in areas of vertical crustal fields and for which Figure 1c is an archetypal example, appearing in one of the strongest field regions of Mars. The spatial overlap between Figures 1a and 1b highlights temporal variability in this crustal field aurora over the 15 min between Swath 1 and Swath 2. Figure 1d through Figure 1f show further examples of this type of aurora for moderate-strength crustal fields. As demonstrated in Figure 3, occurrence rates range from ~20% to 45% in these regions. Emission in these regions often appears up to 300 km in extent, significantly broader than auroral identifications from IUVS (Schneider et al., 2018) or SPICAM (Bertaux et al., 2005). This is due to EMM's distance from Mars, resulting in pixels ranging from 125 to 300 km at the sub-spacecraft point, and possibly due to EMUS' sensitivity to fainter emissions, which may surround the brightest emission in the areas where the crustal fields are most vertical.

In regions of weaker-to-moderate strength crustal field regions when they are near the dusk terminator, we sometimes see emission appearing to be offset from the vertical field region by up to ~200 km (example in Figure 1d), possibly caused by magnetic field draping and warranting further investigation. Interestingly this behavior is not seen near the dawn terminator (example in Figure 1f).

The second type of discrete aurora is what we call "non-crustal field patchy discrete aurora," that is, dim-to-moderate, broadly dispersed features that appear regularly away from strong crustal fields, consistent with Figure 3. Figures 1g–1i show examples of this type of aurora. The patches are typically quite dim, so their shapes/morphology are uncertain since low counting statistics would blur any sharp edges and they may have in reality.

The third and most striking of the auroral features thus far observed by EMUS are shown in Figures 1j–1l. These we are calling "sinuous discrete aurora," due to their thin, elongated, and sometimes serpentine shapes. They share several key traits: (a) they appear in the northern hemisphere away from strong crustal fields, (b) they usually connect to the dayside in the far north but also sometimes separately at lower latitudes, (c) they extend for thousands of kilometers into the night side, (d) they appear on both dusk and dawn sides, and (e) their shapes change moderately and brightnesses shift by factors of up to two over timescales of ~20 min (i.e., the time between swaths, as shown in the differences between Figures 1j and 1k). Given their shapes, one possible explanation is that we are seeing a projection of the magnetotail current sheet onto the nightside atmosphere: electrons are being accelerated toward the planet by current sheet magnetic reconnection (Harada et al., 2017). Their quasi-linear morphology is reminiscent of trans-polar arcs in Earth's polar cap (also called theta aurora (Frank et al., 1986; Peterson & Shelley, 1984)), short-lived features caused by transient plasma convection following a change from northeastward to northwestward IMF or vice versa (Tanaka et al., 2004). It is left to future work to study the behavior and external dependencies of Martian sinuous discrete aurora in detail and to test hypotheses for the mechanisms governing the formation and variability of these enigmatic structures.

5. EUV/FUV Spectra of Mars Aurora

EMUS has measured the first disk-averaged spectrum of Mars' discrete aurora in the FUV (~110–180 nm) and the first auroral spectrum of any kind in the EUV (<110 nm) at Mars (Figure 4). We define auroral and non-auroral nightside (SZA >120°) pixels as those with 130.4 nm emission greater than 3 R and less than 2 R, respectively. These thresholds are imperfect since both resonance fluorescence and aurora contribute to 130.4 nm brightness, with the former occasionally exceeding 3 R, and the latter ranging below 2 R. However, the great majority of pixels comprising coherent structures in Figure 1c are above 3 R. Figure 4, thus, shows mean spectra from both auroral and non-auroral pixels.

First, we notice the non-auroral (mostly airglow) features emitted by the hydrogen exosphere at 102.6 nm (Ly-β) and 121.6 nm (Ly-α) plus an optical ghost peak of Ly-a around 163 nm. In the aurora spectrum, we see the
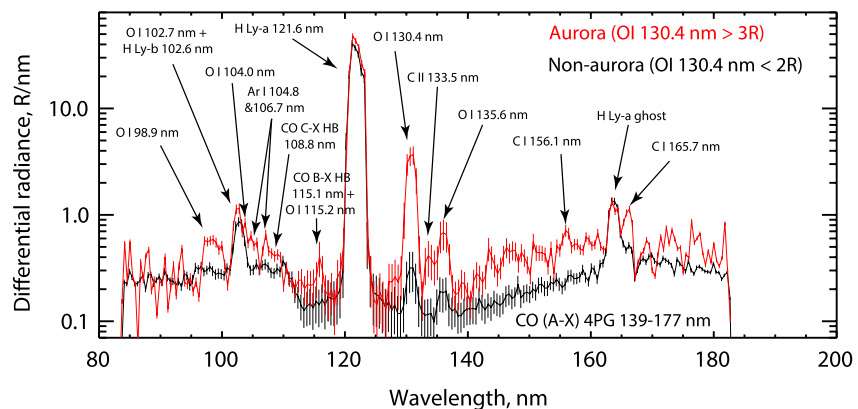
Figure 4. Mean emission spectra from nightside pixels (SZA >120°) in the image shown in Figure 1c (i.e., 28 August 2021). Black represents 6831 pixels with emission at 130.4 nm of <2 R. Red represents 909 pixels with 130.4 nm emission of >3 R.

130.4 nm oxygen emission is > 5 more enhanced relative to a number of weaker but significant oxygen features at 98.9 nm, 102.7 nm (visible above the H Ly-b line), 104.0 nm, and 135.6 nm. Another O line at 115.2 nm overlaps with Hopfield-Birge (HB) B-X emission from CO at 115.1 nm. Further CO emission is visible in the HB C-X emission at 108.8 nm and the CO fourth positive group band system from 139 to 177 nm. In addition, we can identify at least three emissions from excited electronic states of atomic carbon at 133.5 nm, 156.1 nm, and 165.7 nm. These emissions are all consistent with electron impact dissociative excitation of CO_2, resulting in a range of excited states of C, O, and CO. We can further pick out possible Ar I emissions at 104.8 and 106.7 nm. Line/band identification was aided by comparison with the dayside-dominated disk EUV/FUV spectra reported by Krasnopolsky and Feldman (2002) and Feldman et al. (2011).

Similar spectra to Figure 4 are seen for most instances of discrete aurora observed by EMUS, though significant variability (analysis left to future work) is present. Such differences could be used, in concert with electron transport modeling, to constrain differences in the shape of the precipitating electron spectrum, as has been demonstrated by Østgaard et al. (2001).

6. Summary and Conclusions

In this study, we presented the first measurements of extreme UV aurora and the first images of far UV aurora at Mars by the Emirates Mars Mission EMUS instrument. We describe the data set, the method of making images, and the sources of background present in the brightest aurora feature at 130.4 nm. We show that detectable aurorae occur in >~75% of observations. The brightest aurora appear where crustal magnetic fields are both strong and vertical, while the most frequent aurora appear both in these regions and where the crustal fields are very weak or nonexistent. We categorized discrete auroral morphology into three types: crustal field, non-crustal field patchy, and a new unexpected type we call "sinuous," an elongated serpentine structure that stretches thousands of kilometers into the nightside from near midnight in the northern hemisphere and which may be related to the magnetotail current sheet. Lastly, we show the first disk-averaged spectrum of discrete FUV aurora and first ever EUV spectrum of Mars' aurora, with several O, C, and CO features as expected for electron impact primarily on CO_2.

This dataset promises to contribute greatly to our understanding of Mars' magnetospheric dynamics as it provides a synoptic perspective of the locations where electrons deposit energy in the nightside atmosphere. It will complement in situ measurements of particles and fields, both in the upstream solar wind and in the magnetotail, by MAVEN and MEx, as well as limb and disk UV measurements by MAVEN IUVS. This powerful combination of measurements promises to assist in unraveling the chain of cause-and-effect, and the role of Mars' crustal fields, as solar wind energy and momentum is transferred to and throughout Mars' unique magnetosphere.

Data Availability Statement

Data from the Emirates Mars Mission (EMM) are freely and publicly available on the EMM Science Data Center (SDC, http://sdc.emiratesmarsmission.ae). This location is designated as the primary repository for all data products produced by the EMM team and is designated as long-term repository as required by the UAE Space Agency. The data available (http://sdc.emiratesmarsmission.ae/data) include ancillary spacecraft data, instrument telemetry, Level 1 (raw instrument data) to Level 3 (derived science products), quick look products, and data users guides (https://sdc.emiratesmarsmission.ae/documentation) to assist in the analysis of the data. Following the creation of a free login, all EMM data are searchable via parameters such as product file name, solar longitude, acquisition time, sub-spacecraft latitude and longitude, instrument, data product level, etc. Emirates Mars Ultraviolet Spectrograph (EMUS) data and users guides are available at: https://sdc.emiratesmarsmission.ae/data/emus. The MAVEN EUVM L3 data are publicly available at the NASA planetary data system through https://pds-ppi.igpp.ucla.edu/search/view?f=yes&id=pds://PPI/maven.euv.modelled.

References

Amiri, H. E. S., Brain, D., Sharaf, O., Withnell, P., McGrath, M., Alloghani, M., et al. (2022). The Emirates Mars mission. *Space Science Reviews*, *218*(1). https://doi.org/10.1007/s11214-021-00868-x

Bertaux, J. L., Leblanc, F., Witasse, O., Quemerais, E., Lilensten, J., Stern, S. A., et al. (2005). Discovery of an aurora on Mars. *Nature*, *435*(7043), 790–794. https://doi.org/10.1038/nature03603

Brain, D. A., Halekas, J. S., Peticolas, L. M., Lin, R. P., Luhmann, J. G., Mitchell, D. L., et al. (2006). On the origin of aurorae on Mars. *Geophysical Research Letters*, *33*(1). https://doi.org/10.1029/2005gl024782

Brain, D. A., Lillis, R. J., Mitchell, D. L., Halekas, J. S., & Lin, R. P. (2007). Electron pitch angle distributions as indicators of magnetic field topology near Mars. *Journal of Geophysical Research-Space Physics*, *112*(A9). https://doi.org/10.1029/2007ja012435

Chafflin, M., Fowler, C. M., Deighan, J., Jain, S., Holsclaw, G., Hughes, A., et al. (2022). Patchy proton aurora at Mars: A global view of solar wind precipitation across the Martian dayside from EMM/EMUS. *Geophysical Research Letter*, *49*, e2022GL099881. https://doi.org/10.1029/2022GL099881

Deighan, J., Chaffin, M. S., Chaufray, J. Y., Stewart, A. I. F., Schneider, N. M., Jain, S. K., et al. (2015). MAVEN IUVS observation of the hot oxygen corona at Mars. *Geophysical Research Letters*, *42*(21), 9009–9014. https://doi.org/10.1002/2015gl065487

Deighan, J., Jain, S. K., Chaffin, M. S., Fang, X., Halekas, J. S., Clarke, J. T., et al. (2018). Discovery of a proton aurora at Mars. *Nature Astronomy*, *2*(10), 802–807. https://doi.org/10.1038/s41550-018-0538-5

Edwards, C. S., Christensen, P. R., Mehall, G. L., Anwar, S., Tunaiji, E. A., Badri, K., et al. (2021). The Emirates Mars mission (EMM) Emirates Mars InfraRed spectrometer (EMIRS) instrument. *Space Science Reviews*, *217*(7). https://doi.org/10.1007/s11214-021-00848-1

Fang, X., Ma, Y., Schneider, N., Girazian, Z., Luhmann, J., Milby, Z., et al. (2022). Discrete aurora on the nightside of Mars: Occurrence location and probability. *Journal of Geophysical Research: Space Physics*, *127*(3), e2021JA029716. https://doi.org/10.1029/2021ja029716

Feldman, P. D., Steffl, A. J., Parker, J. W., A'Hearn, M. F., Bertaux, J.-L., Alan Stern, S., et al. (2011). Rosetta-Alice observations of exospheric hydrogen and oxygen on Mars. *Icarus*, *214*(2), 394–399. https://doi.org/10.1016/j.icarus.2011.06.013

Frank, L. A., Craven, J. D., Gurnett, D. A., Shawhan, S. D., Weimer, D. R., Burch, J. L., et al. (1986). The theta-aurora. *Journal of Geophysical Research-Space Physics*, *91*(A3), 3177–3224. https://doi.org/10.1029/JA091iA03p03177

Gérard, J.-C., Soret, L., Libert, L., Lundin, R., Stiepen, A., Radioti, A., & Bertaux, J. L. (2015). Concurrent observations of ultraviolet aurora and energetic electron precipitation with Mars Express. *Journal of Geophysical Research: Space Physics*, *120*(8), 6749–6765. https://doi.org/10.1002/2015JA021150

Gerard, J. C., Soret, L., Shematovich, V. I., Bisikalo, D. V., & Bougher, S. W. (2017). The Mars diffuse aurora: A model of ultraviolet and visible emissions. *Icarus*, *288*, 284–294. https://doi.org/10.1016/j.icarus.2017.01.037

Girazian, Z., Schneider, N. M., Milby, Z., Fang, X., Halekas, J., Weber, T., et al. (2022). Discrete aurora at Mars: Dependence on upstream solar wind conditions. *Journal of Geophysical Research: Space Physics*, *127*(4), e2021JA030238. https://doi.org/10.1029/2021JA030238

Harada, Y., Halekas, J. S., McFadden, J. P., Espley, J., DiBraccio, G. A., Mitchell, D. L., et al. (2017). Survey of magnetic reconnection signatures in the Martian magnetotail with MAVEN. *Journal of Geophysical Research: Space Physics*, *122*(5), 5114–5131. https://doi.org/10.1002/2017JA023952

Holsclaw, G., Deighan, J., Almatroushi, H., Chaffin, M., Evans, S., Fillingim, M., et al. (2021). The Emirates ultraviolet spectrometer (EMUS) for the EMM mission. *Advances in Space Research*.

Hughes, A., Chaffin, M., Mierkiewicz, E., Deighan, J., Jain, S., Schneider, N., et al. (2019). Proton aurora on Mars: A dayside phenomenon pervasive in southern summer. *Journal of Geophysical Research: Space Physics*, *124*(12), 10533–10548. https://doi.org/10.1029/2019JA027140

Krasnopolsky, V. A., & Feldman, P. D. (2002). Far ultraviolet spectrum of Mars. *Icarus*, *160*(1), 86–94. https://doi.org/10.1006/icar.2002.6949

Langlais, B., Thebault, E., Houliez, A., Purucker, M. E., & Lillis, R. J. (2019). A new model of the crustal magnetic field of Mars using MGS and MAVEN. *Journal of Geophysical Research-Planets*, *124*(6), 1542–1569. https://doi.org/10.1029/2018je005854

Leblanc, F., Witasse, O., Lilensten, J., Frahm, R. A., Safaenili, A., Brain, D. A., et al. (2008). Observations of aurorae by SPICAM ultraviolet spectrograph on board Mars Express: Simultaneous ASPERA-3 and MARSIS measurements. *Journal of Geophysical Research*, *113*(A8). https://doi.org/10.1029/2008ja013033

Leblanc, F., Witasse, O., Winningham, J., Brain, D., Lilensten, J., Blelly, P. L., et al. (2006). Origins of the martian aurora observed by spectroscopy for investigation of characteristics of the atmosphere of Mars (SPICAM) on board Mars express. *Journal of Geophysical Research*, *111*(A9). https://doi.org/10.1029/2006ja011763

Lillis, R. J., Frey, H. V., Manga, M., Mitchell, D. L., Lin, R. P., Acuna, M. H., & Bougher, S. W. (2008). An improved crustal magnetic field map of Mars from electron reflectometry: Highland volcano magmatic history and the end of the martian dynamo. *Icarus*, *194*(2), 575–596. https://doi.org/10.1016/j.icarus.2007.09.032

Nakamura, Y., Terada, N., Leblanc, F., Rahmati, A., Nakagawa, H., Sakai, S., et al. (2022). Modeling of diffuse auroral emission at Mars: Contribution of MeV protons. *Journal of Geophysical Research: Space Physics*, *127*(1), e2021JA029914. https://doi.org/10.1029/2021JA029914

Østgaard, N., Stadsnes, J., Bjordal, J., Germany, G. A., Vondrak, R. R., Parks, G. K., et al. (2001). Auroral electron distributions derived from combined UV and X-ray emissions. *Journal of Geophysical Research*, *106*(A11), 26081–26089. https://doi.org/10.1029/2001JA000031

Peterson, W. K., & Shelley, E. G. (1984). Origin of the plasma in a cross-polar cap auroral feature (Theta-Aurora). *Journal of Geophysical Research-Space Physics*, *89*(A8), 6729–6736. https://doi.org/10.1029/JA089iA08p06729

Ritter, B., Gérard, J.-C., Hubert, B., Rodriguez, L., & Montmessin, F. (2018). Observations of the proton aurora on Mars with SPICAM on board Mars express. *Geophysical Research Letters*, *45*(2), 612–619. https://doi.org/10.1002/2017GL076235

Schneider, N. M., Deighan, J. I., Jain, S. K., Stiepen, A., Stewart, A. I. F., Larson, D., et al. (2015). Discovery of diffuse aurora on Mars. *Science*, *350*(6261).

Schneider, N. M., Jain, S. K., Deighan, J., Nasr, C. R., Brain, D. A., Larson, D., et al. (2018). Global aurora on Mars during the September 2017 space weather event. *Geophysical Research Letters*, *45*(15), 7391–7398. https://doi.org/10.1029/2018gl077772

Schneider, N. M., Milby, Z., Jain, S. K., Gérard, J. C., Soret, L., Brain, D. A., et al. (2021). Discrete aurora on Mars: Insights into their distribution and activity from MAVEN/IUVS observations. *Journal of Geophysical Research: Space Physics*, *126*(10), e2021JA029428. https://doi.org/10.1029/2021JA029428

Soret, L., Gerard, J. C., Libert, L., Shematovich, V. I., Bisikalo, D. V., Stiepen, A., & Bertaux, J. L. (2016). SPICAM observations and modeling of Mars aurorae. *Icarus*, *264*, 398–406. https://doi.org/10.1016/j.icarus.2015.09.023

Soret, L., Gérard, J.-C., Schneider, N., Jain, S., Milby, Z., Ritter, B., et al. (2021). Discrete aurora on Mars: Spectral properties, vertical profiles, and electron energies. *Journal of Geophysical Research: Space Physics*, *126*(10), e2021JA029495. https://doi.org/10.1029/2021JA029495

Tanaka, T., Obara, T., & Kunitake, M. (2004). Formation of the theta aurora by a transient convection during northward interplanetary magnetic field. *Journal of Geophysical Research-Space Physics*, *109*(A9). https://doi.org/10.1029/2003ja010271

Xu, S. S., Mitchell, D. L., McFadden, J. P., Schneider, N. M., Milby, Z., Jain, S., et al. (2022). Empirically determined auroral electron events at Mars-MAVEN observations. *Geophysical Research Letters*, *49*(6). https://doi.org/10.1029/2022GL097757

References From the Supporting Information

Hanson, W. B., Sanatani, S., & Zuccaro, D. R. (1977). The Martian ionosphere as observed by the Viking retarding potential analyzers. *Journal of Geophysical Research*, *82*(28), 4351–4363. https://doi.org/10.1029/JS082i028p04351

Ip, W. H. (1988). On a hot oxygen corona of Mars. *Icarus*, *76*(1), 135–145. https://doi.org/10.1016/0019-1035(88)90146-7

McElroy, M. B., & Donahue, T. M. (1972). Stability of the martian atmosphere. *Science*, *177*(4053), 986–988. https://doi.org/10.1126/science.177.4053.986

Thiemann, E. M. B., Chamberlin, P. C., Eparvier, F. G., Templeman, B., Woods, T. N., Bougher, S. W., & Jakosky, B. M. (2017). The MAVEN EUVM model of solar spectral irradiance variability at Mars: Algorithms and results. *Journal of Geophysical Research-Space Physics*, *122*(3), 2748–2767. https://doi.org/10.1002/2016ja023512